Overall Crystallization Behavior of Polypropylene–Clay Nanocomposites; Effect of Clay Content and Polymer/Clay Compatibility on the Bulk Crystallization and Spherulitic Growth

C. J. Perez, V. A. Alvarez

Research Institute of Material Science and Technology (INTEMA), National University of Mar del Plata (UNMdP), 7600 Mar del Plata, Argentina

Received 24 October 2008; accepted 9 March 2009
DOI 10.1002/app.30395
Published online 7 August 2009 in Wiley InterScience (www.interscience.wiley.com).

ABSTRACT: The effect of clay nanoparticles on the overall crystallization (isothermal crystallization, spherulitic growth, and nonisothermal crystallization) behavior of polypropylene (PP) was studied by means of differential scanning calorimetry and polarized light optical microscopy. In addition, the changes produced by the compatibility between the filler and the matrix were analyzed by using more hydrophobic clays or incorporating PP grafted with maleic anhydride (PP-*g*-MA). Different models were used to predict the relative degree of crystallinity and several parameters were analyzed. A clear nucleating effect of clay nanoparticles was found on the experimental behavior (induction time, half-crystallization time, and overall crystallization time) and also deducted from the models parameters (Avrami exponent, rate constant, nucleation activity, activation energy). The effect was also related with the matrix/clay compatibility. In addition, the polarized light optical microscopy showed that the number of spherulites increased and their size decreased when clay was incorporated, which is also an indication of the heterogeneous nucleating behavior of such particles. We also noted faster spherulitic growth and increasing K_g (the model parameter). © 2009 Wiley Periodicals, Inc. J Appl Polym Sci 114: 3248–3260, 2009

Key words: nanocomposites; modeling; crystallization; spherulitic growth; compatibility; model parameters

INTRODUCTION

Although there are several studies on the crystallization behavior of clay/polymeric matrix nanocomposites, different and sometimes contradictory results have been reported about the effect of nanoparticles on the crystallization behavior of semicrystalline polymers,[1,2] which is very important because the final properties depend on it. In addition, only few works are related to the spherulite growth.

Several authors have demonstrated the nucleating and accelerating effects of clay nanoparticles by analyzing different experimental parameters: the increase on the crystallization temperature (T_c) with respect to the neat matrix,[3,4] the increase on the melting and crystallization temperatures (T_m and T_c),[5] the higher crystallization rate,[6,7] the reduction of the effective energy barrier,[6] and the decrease in the half-crystallization time.[8–10]

This accelerating behavior was also demonstrated by means of models parameters, for example, the activation energy from Kissinger model, i.e., the higher the clay content the lower, meanwhile, the activation energy,[10] and the parameters of Mo's equation.[8–10]

There is another controversial point related with the applicability of different models; however, some authors[10] claimed that both traditional methods, Avrami and Ozawa, were inapplicable, whereas Mo's model was adequate to describe the nonisothermal crystallization behavior of PP/clay nanocomposites; other authors[6] also stated that Ozawa's was nonapplicable but Avrami's gave satisfactory results for the modeling of the nonisothermal crystallization of PP/clay nanocomposites. Nevertheless, diverse and sometimes incongruous results[6,9,11] with respect to the parameters of those models were found. An additional complication came from the fact that some authors have claimed that the nucleating effect depends on the cooling rate.[12]

Another contradiction is related to the use of different clay (unmodified and modified, mainly to make it more compatible with the hydrophobic thermoplastic matrix) in the same matrix, whereas some studies[13] indicate that the higher the dispersion degree (higher matrix/clay compatibility), the lower becomes the clay nucleation effect; another ones[9] correlate the nucleation effect with the contact area between

Correspondence to: V. A. Alvarez (alvarezvera@fi.mdp.edu.ar).

Contract grant sponsor: ANPCyT; contract grant numbers: PICT 22-25766, PICT 05-32379.

Contract grant sponsor: National Research Council of Argentina (CONICET).

TABLE I
Equations Used for the Modeling of Crystallization Process

	Equations	Parameters	Ref.
Degree of crystallinity	$X_{cr}(\%) = \frac{\Delta H_f}{w_{PP} \times \Delta H_{100}} \times 100$	ΔH_f: experimental heat of fusion w_{PP}: PP weight fraction and ΔH_{100}: heat of fusion of 100% crystalline PP (207.1 J/g)	23
		Isothermal crystallization	
Relative degree of crystallinity	$\alpha = \frac{\int_0^t \frac{dH}{dt}.dt}{\int_0^\infty \frac{dH}{dt}.dt} = \frac{\Delta H_t}{\Delta H_0}$	ΔH_t: heat generated at time t ΔH_0: total heat generated up to the complete crystallization	24
Avrami's model	$\alpha = 1 - \exp(-k \cdot t^n)$	k: Avrami rate constant (containing the nucleation and the growth parameters) n: Avrami exponent (depends on the mechanism of nucleation and on the form of crystal growth)	25
Rate constant	$k = \frac{\ln 2}{t_{1/2}^n}; \sqrt[n]{\frac{k}{\ln 2}} = \frac{1}{t_{1/2}} = \text{OCR}$	$t_{1/2}$: half-crystallization time (time at which the relative degree of crystallinity approaches 0.5) OCR: overall crystallization rate	
Arrhenius's equation	$k = k_0 \cdot \exp\left(-\frac{E_a}{R(T_m^0 - T_c)}\right)$	k_0: preexponential factor R: universal gas constant E_a: total activation energy T_m^0: theoretical melting point; T_c: crystallization temperature	26
Hoffman-Weeks method	T_m^0 is obtained from the interception of $T_m = f(T_c)$ with $T_m = T_c$	T_m: melting temperature T_c: crystallization temperature	27
Induction time	$t_i = K_{t_i} \cdot \exp\left(\frac{E_{t_i}}{R\Delta T}\right)$	t_i: induction time (time needed for the formation of the equilibrium nucleus with critical dimensions at a given T) K_{ti}: preexponential factor for the nucleation process K_{ti}: activation energy for the nucleation process	28
		Spherulitic growth	
Spherulitic growth rate	$G(T) = G_0 \cdot \exp\left(-\frac{U^*}{R(T_c - T_\infty)}\right) \times \exp\left(-\frac{K_g}{T_c \cdot \Delta T \cdot f}\right)$	G_0: preexponential factor U^*: activation energy for segmental jump rate in polymers (1500 cal/mol) R: universal gas constant T_c: crystallization temperature $T_\infty = T_g - 30$ K $f = \frac{2 \cdot T_c}{T_c + T_m^0}$	29
		Nonisothermal crystallization	
Relative degree of crystallinity	$\alpha = \frac{\int_0^T \frac{dH}{dT}.dT}{\int_0^\infty \frac{dH}{dT}.dT}$	T_0: onset crystallization temperature T_∞: final crystallization temperature; H_c: crystallization enthalpy	
Avrami's model	$1 - \alpha = \exp(Z_t t^n)$	Z_t: rate constant in the nonisothermal crystallization process	30
Nucleation activity	$\varepsilon = \frac{B_f}{B_0}$	ε: nucleation activity of the filler B_f: slope of log ϕ vs. $1/2.3\Delta T_p^2$ curve for nanocomposite B_0: idem for the matrix $\Delta T_p = T_m - T_p$ (peak temperature)	31
Kinetic parameter	$\log Z_c = \frac{\log Z_t}{\phi}$	ϕ: cooling rate Z_c: parameter characterizing the kinetic of nonisothermal crystallization	32
Ozawa's model	$1 - \alpha = \exp\left(\frac{-K(T)}{\phi^m}\right)$	$K(T)$: function of cooling rate M: Ozawa exponent (depends on the crystal growth)	33
Mo's model	$\ln \phi = \ln F(T) - b \ln t$	$F(T) = [K(T)/Z_t]^{1/m}$ represents the value of cooling rate (must be chosen within the unit crystallization time when the measured system amounted to a certain degree of crystallinity) b: (m/n) ratio of the Avrami exponent n to the Ozawa exponent	34
Kissinger's model	$\frac{d\left[\ln\left(\phi/T_p^2\right)\right]}{d\left(1/T_p\right)} = \frac{-\Delta E_T}{R}$	T_p: crystallization peak temperature ΔE_T: activation energy for the transport of the macromolecular segments to the growing surface	35

polymer segments and clay surface, i.e., a higher contact area resulting from the higher clay interlayer spacing produces a greater nucleation effect.

In addition, to improve the compatibility, maleic anhydride-*grafted*-polypropylene (PP-*g*-MA) can be used. In this case, the studies are in accordance with the first approach; PP/PP-*g*-MA/clay systems containing the clay tactoids crystallized faster, whereas no nucleation ability in systems with well-dispersed clay was observed.[14] In this case, another effect should be taken into account: the use of PP-*g*-MA compatibilizer contributes to the retardation of the quiescent isothermal crystallization kinetics relative to the neat PP.[14]

Analyzing the spherulitic growth, a reduction of the spherulites size by the addition of the nanofiller is generally found, either due to the higher amount of crystalline defects caused by the presence of the particles[15] or to the nucleating effect of those particles.[16,17]

Bulk crystallization and spherulitic growth not always follow a similar trend. Some authors have probed that whereas the nanoparticles serve as nucleation agent resulting in an enhancement of the overall crystallization rate (OCR), a constant spherulite growth rate is observed, suggesting that nucleation and growth of spherulites are two independent processes.[18,19] However, other authors[20] have found an increasing trend on the spherulitic growth rate and, opposite, other studies[21,22] have demonstrated that silica increased the crystallization rate of pure polymeric matrices but decreased the spherulite growth rate because of the viscosity increment, which decreased the transport of crystallizable chains to the crystal front. A further point is related to the matrix/clay compatibility: the higher the matrix/clay miscibility, the slower is the bulk crystallization and the faster is the spherulitic growth.[13]

The aim of this work was to study and model the overall crystallization process (isothermal, nonisothermal, and spherulitic growth) of PP reinforced with nanoclay and to analyze the effect of clay content and the clay/matrix compatibility (by changing the clay and also by incorporating PP-*g*-MA as compatibilizer) on the experimental behavior and parameters obtained from several models with respect to the neat PP. The models and equations used in this work are summarized in Table I. Also, the usefulness of each model will be analyzed.

EXPERIMENTAL

Materials

Isotactic PP supplied by Petroquímica Cuyo, Mendoza, Argentina, was used as a matrix. Some of its physical and mechanical properties are shown in Table II. To improve the compatibility between PP matrix and clay, 10 wt % PP-*g*-MA (Epolene E-43 wax, Eastman Chemical Company, Kingsport, TN) was also added in the formulation of some nanocomposites.

TABLE II
Physical and Mechanical Properties of the Polypropylene Matrix (Technical Datasheet)

Melt flow index (230°C/2.16 kg)	3.4 g/10 min
Young's modulus	1.45 GPa
Melting point	166°C
Density	0.88–0.92 g/cm^3

Three different commercially available clays [Cloisite Na^+ (MMT), Cloisite 30B® (C30B), and Cloisite 10A® (C10A), purchased from Southern Clay Products, Austin, TX] were employed as nanofillers. They were used as received. Their characteristics are shown in Table III.

Nanocomposites preparation

The nanocomposites were prepared in an intensive mixer (Brabender type) at 180°C; the speed of rotation and the mixing time were 50 rpm and 10 min, respectively. Different MMT contents (0.5, 1, 3, and 5 wt%) were used. After mixing, 3-mm plaques were compression molded in a hydraulic press for 10 min at 180°C under a pressure of 50 kg/cm^2. Once the effect of clay content was studied, the initial materials were changed.

- 10 wt % of PP-*g*-MA was incorporated in the matrix of PP/5 wt % MMT nanocomposites.
- 5 wt % of C10A or C30B were used as reinforcement instead of MMT for the neat PP.

Methods

Transmission electron microscopy

Transmission electron microscope (TEM) JEOL CX II using an acceleration voltage of 80 kV was used to observe the dispersion of clay platelets within the polymer chains.

Differential scanning calorimetry

A differential scanning calorimeter (DSC Perkin Elmer 7) was used to study the isothermal and nonisothermal crystallization processes. Samples of about 10 mg were accurately weighted. All DSC analyses were performed under nitrogen atmosphere. In both cases, a first run was done from room temperature to 200°C at a heating rate of 10°C/min. Then, the samples were melted for 5 min at 200°C to permit the complete melting of the crystals.

TABLE III
Characteristics of the Different Nanoclays Used

Clay	Organic modifier	Modifier concentration (mequiv/100 g clay)	Specific gravity (g/cm^3)
MMT	None		2.86
C30B	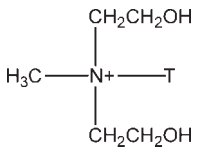	90	1.98
C10A	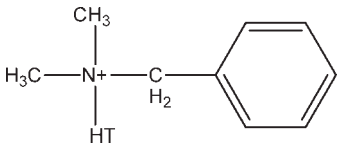	125	1.90

Isothermal crystallization. Then, the samples were cooled to the crystallization temperature at 30°C/min and maintained at the crystallization temperature for 30 min to allow complete crystallization. The material was crystallized in the temperature range of 124–128°C. Then, the sample was heated from the crystallization temperature to 200°C at 10°C/min to melt the crystals formed at the crystallization temperature and to find the melting temperature of each material. The degree of crystallinity was almost constant (41 ± 2%) for the matrix and all nanocomposites. A similar value and behavior was found by other authors.[36,37] This is an expected behavior because the nucleation of MMT would increase the relative degree of crystallinity slightly because only a small portion of MMT had an effect on the nucleation,[38,39] whereas most of the MMT layers restricted the motion of PP chains; the restricted chains might not crystallize decreasing the crystallization degree.

Nonisothermal crystallization. The samples were cooled to room temperature at different cooling rates (5, 10, 15, 20, and 25°C/min).

Transmission optical microscopy

An optical microscopy Leica DM LB with a hot-stage Linkam THMS 600 was used for the test. Samples were prepared by cutting small pieces from films. These samples were heated from room temperature to 200°C at 10°C/min, kept for 10 min at 200°C, and then quickly cooled to the crystallization temperature (between 138 and 144°C). Then, they were maintained at each temperature for at least 10 min. Polarized light was used to observe the spherulites morphology. Images of the spherulites were taken at several times and their radii were measured by using a software tool. The time-lapsed frames were recorded to determine the spherulitic growth rate.

RESULTS AND DISCUSSION

Bulk isothermal crystallization

During isothermal crystallization, an increase of the melting temperature (T_m) as a function of crystallization temperature (T_c) was observed for the matrix and also for all nanocomposites. This behavior was probably related with the increase on the chains mobility when crystallization temperature increased.[40] From the fusion temperatures after each crystallization step, T_m^0 (thermodynamic melting point) was determined by the Hoffman-Weeks method as shown in Figure 1 for PP matrix. T_m^0 was almost constant (182°C), and in the range obtained from literature,[41–43] for the matrix and MMT nanocomposites. This results drives to the idea that nanoclay particles does not have an important effect on the perfection of PP crystallites. Nevertheless, other authors[17,44]

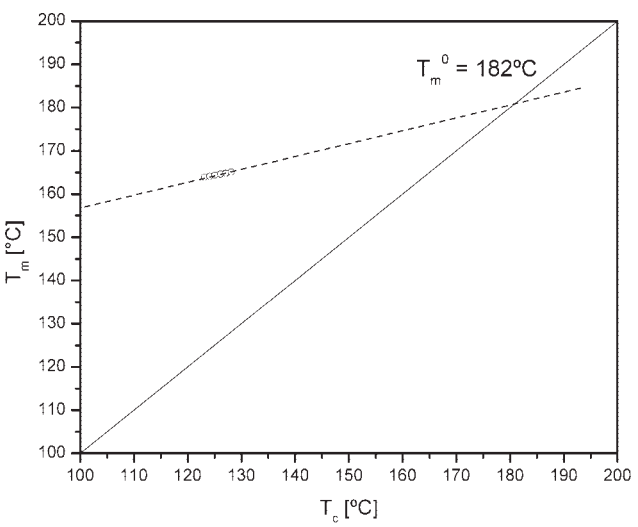

Figure 1 Hoffman-Weeks plot for PP matrix. Determination of the thermodynamic melting point (T_m^0).

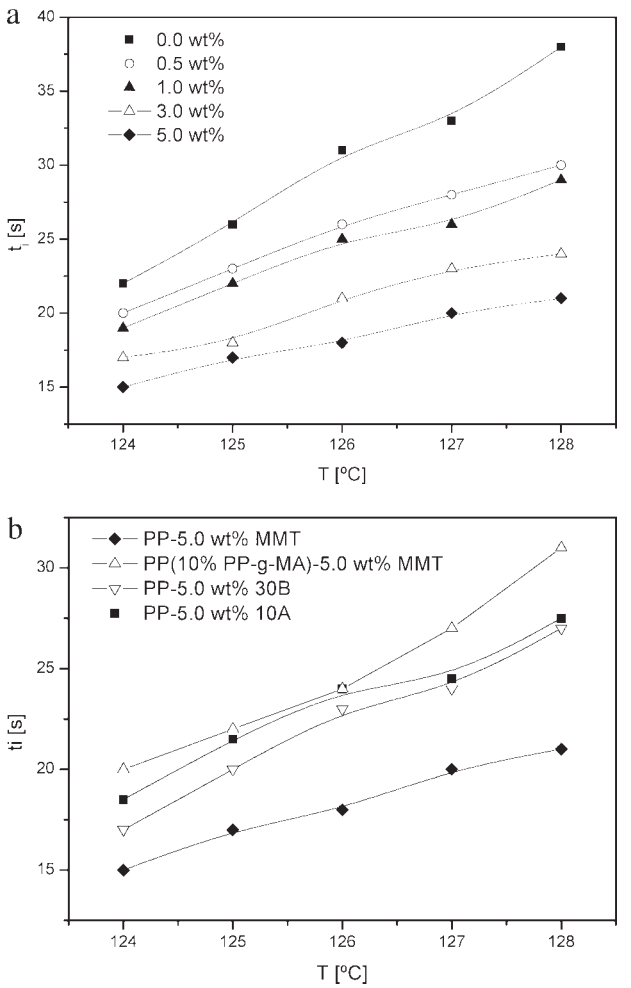

Figure 2 Induction time as a function of crystallization temperature for (a) PP-matrix and nanocomposites with different MMT contents and (b) nanocomposites with modified initial materials: PP-5 wt % C30B; PP-5 wt % C10A, and PP(10% PP-*g*-MA)-5 wt % MMT.

have found an increasing trend on the theoretical melting point as a function of the nanofiller content. In our case, different theoretical melting points were found for modified systems: PP/C10A (189.3°C), PP/C30B (180°C), and PP/PP-*g*-MA/MMT (185.4°C).

Nucleation process

Figure 2 shows the relationship between the induction time and the crystallization temperature for PP matrix and the nanocomposites with different MMT contents (a) and with different initial materials (b). Independently of the clay content and additives used, induction time increased with crystallization temperature because of the decrease on the undercooling degree, which is the driving force for crystallization process.

From Figure 2(a) it is clear that the induction time decreased as a function of clay content because spherulites need less time to heterogeneously nucleate; so, they act as nucleating agents. Heterogeneous nucleation took place in the nanocomposites, whereas homogeneous/heterogeneous nucleation occurs in the case of pure matrix. Homogeneous nucleation begins suddenly by chain aggregation below the melting point needing more time to reach the maximum crystallization rate.[17] On the other hand, Figure 2(b) shows the higher induction times for PP-5 wt % C30B, PP-5 wt % C10A, and PP-5 wt % MMT-PP-*g*-MA (with respect to PP-5 wt % MMT), which is related to the upper compatibility between the modified clays (which are both more hydrophobic than the original one) with the matrix and to the compatibilization between PP-*g*-MA and MMT in accordance to Krikorian et al.[13]

As the matrix is hydrophobic and MMT is hydrophilic, there is necessary to improve the interactions between both of them.[45–47] For this purpose, there are two options: to functionalize the polymer by the addition of functional oligomers using, for example, PP-*g*-MA, and the other is to modify the clay. TEM images (Fig. 3) confirmed this behavior and are in accordance with the results obtained for the induction time. In view of the fact that the silicate platelets are dark, the presence of tactoids whose are unseparated montmorillonite layers is manifested and there are some regions where a small amount of polymer occupied the intragallery spacing [Fig. 3(a)], which is a typical observed morphology when no compatibility exists between clay and PP.[48] It can be observed from Figure 3(b,c) that the dispersion of clay nanoparticles in the PP matrix was enhanced where modified clays were used; especially for the clay C10A, which is the most hydrophobic (highest polymer–clay compatibility). Moreover, Figure 3(d) evidence that PP-*g*-MA contributed to a higher degree of disordered structures and exfoliated layers. The mechanical properties previously reported, are also in accordance with the present ones.[49] From the previous results (TEM and induction times), it was concluded that the higher the dispersion degree, the lower is the nucleation effect.[13]

The experimental induction times were modeled by obtaining the preexponential factor, K_{ti}, and the activation energy, E_{ti}, from a typical nonlinear Leberverg-Marquard regression method in the OriginPro 7.5 software. To compare, an average K_{ti} value of 0.1 was used. The results are summarized in Table IV. Activation energy for the induction process decreased with the clay incorporation and as a function of clay content, which in turn indicates that the nucleation process is facilitated by the presence of clay. In the case of modified materials (C10A, C30B, PP-*g*-MA), the value was higher than that of the PP

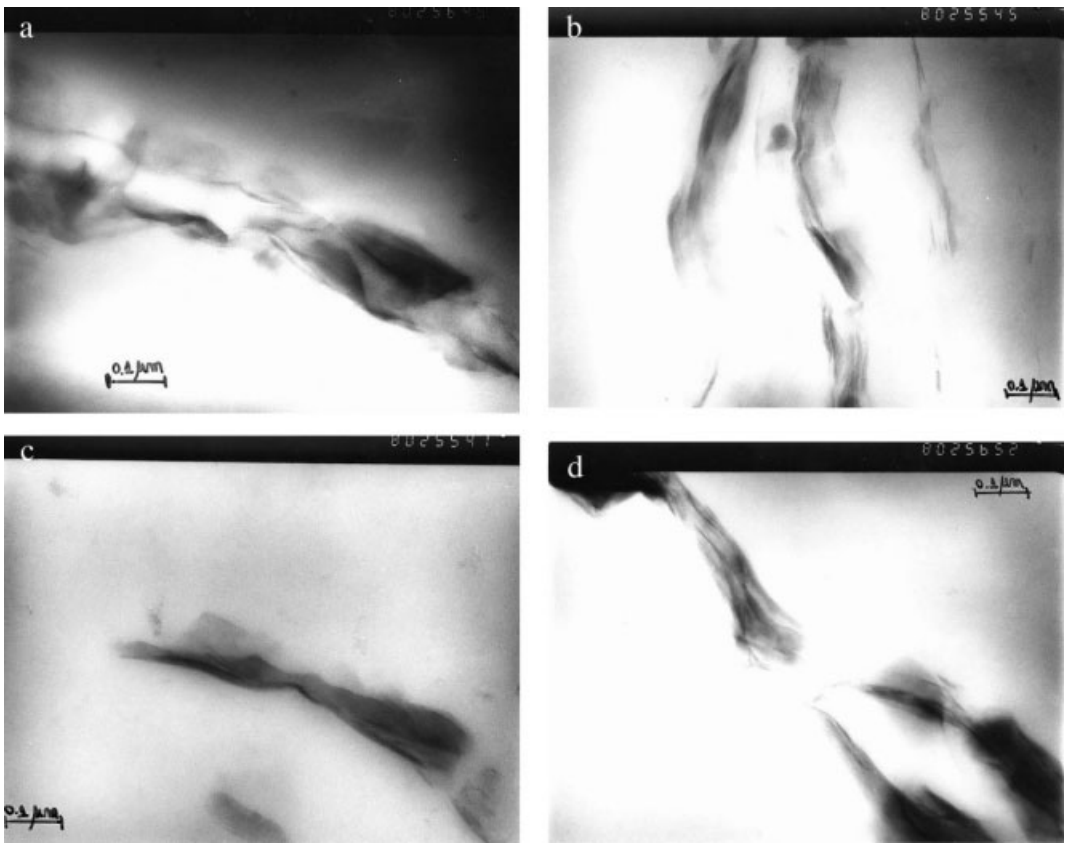

Figure 3 TEM images for (a) PP-5 wt % MMT; (b) PP-5 wt % C10A; (c) PP-5 wt % C30B; and (d) PP(10% PP-*g*-MA)-5 wt % MMT.

5 wt % MMT, which is in accordance with the experimental trend.

Crystal growth process

Figure 4 shows the degree of crystallinity as a function of time (T_c = 128°C) for the matrix and nanocomposites with different MMT contents [Fig. 4(a)] and with different initial materials [Fig. 4(b)]. A clear tendency can be found in Figure 4(a) for clay content, i.e., the higher the MMT concentration, the faster is the crystallization process. On the other hand [Fig. 4(b)], the higher half-crystallization times for the organomodified clay nanocomposites can be attributed to a decreased nucleation effect, which is related to the fact that the dispersed clay platelets may hinder the chain-folding mechanism for local polymeric matrix crystallization.[13,50]

Figure 5 shows the experimental OCR as a function of crystallization temperature for the matrix and nanocomposites with different MMT contents. It can be seen that this parameter decreases as the crystallization temperature becomes higher because of the lower undercooling degree, i.e., the lower

TABLE IV
Parameters of Isothermal Crystallization for Different Materials Studied

	E_{t_i} (K_{t_i}= 0.10) (kJ/mol)	OCR_{exp} (s^{-1})	$OCR_{predict}$ (s^{-1})	n	E_{act} (kJ/mol)
PP	100	2.11×10^{-3}	2.13×10^{-3}	2.38 ± 0.08	808
PP 0.5 wt % MMT	97.0	3.34×10^{-3}	3.28×10^{-3}	2.22 ± 0.08	792
PP 1.0 wt % MMT	96.7	4.15×10^{-3}	4.08×10^{-3}	2.02 ± 0.09	760
PP 3.0 wt % MMT	92.9	5.24×10^{-3}	5.10×10^{-3}	1.86 ± 0.06	745
PP 5.0 wt % MMT	91.1	8.85×10^{-3}	8.62×10^{-3}	2.06 ± 0.26	724
PP(10% PP-*g*-MA) 5.0 wt % MMT	93.9	5.10×10^{-3}	4.65×10^{-3}	2.70 ± 0.10	777
PP 5.0 wt % C30B	94.3	8.78×10^{-3}	8.77×10^{-3}	2.42 ± 0.08	768
PP 5.0 wt % C10A	95.5	6.85×10^{-3}	5.65×10^{-3}	2.24 ± 0.06	783

E_{t_i}: activation energy for nucleation process; OCR (T_c = 128°C): overall crystallization rate at crystallization temperature of 128°C; exp: experimental values; predict: predicted values; n: average Avrami exponent (T_c = 124–128°C); E_{act}: activation energy for crystal growth.

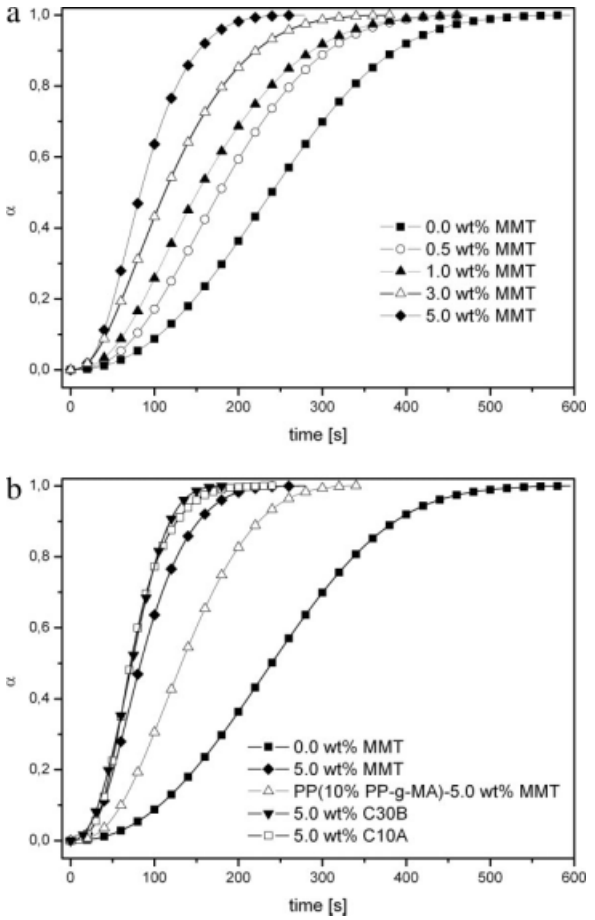

Figure 4 Relative degree of crystallinity (α) as a function of time for (a) PP matrix and nanocomposites with different MMT contents and (b) nanocomposites with modified initial materials: PP-5 wt % C30B; PP-5 wt % C10A; and PP(10% PP-*g*-MA)-5 wt % MMT.

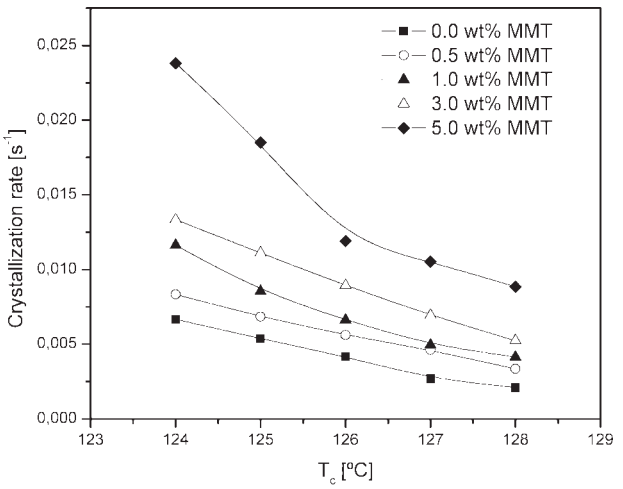

Figure 5 Overall crystallization rate (OCR) as a function of crystallization temperature (T_c) for PP matrix and nanocomposites with different MMT contents.

crystallization driving force. This behavior was also observed for different initial materials. In addition, the nanocomposites crystallized faster than PP matrix because the clay particles serve as additional nucleation sites. Table IV also includes OCR for studied materials. The heterogeneous nucleation effect was lower when the compatibilization between PP and the clay was improved (i.e., C10A, C30B, and incorporation of PP-*g*-MA).

The parameters of Avrami model (Avrami exponent, n, and rate constant, k) were calculated in the range of α between 0.1 and 0.9. The obtained values are summarized in Table V, whereas average values for n are included in Table IV. In the case of the matrix, n was equal to 2.4 ± 0.1.[6,17] On the other hand, the average value for all nanocomposites was near to 2, indicating a two-dimensional crystal growth with a linear growth rate and the crystal nucleating athermally.[51] On the contrary, Wang et al.[16] and Ma et al.[17] have found an increment on n for nanocomposites.

In all cases, the rate constant, k, decreased with the increase of the crystallization temperature. In addition, at a constant temperature k increased when clay was incorporated; this indicates the faster bulk crystallization in comparison with the neat matrix.[6] On the other hand, the change of the original clay for the organoclay or the addition of PP-*g*-MA produced a decrease on k, which is related with

TABLE V
Parameters of Avrami Equation for Matrix and Nanocomposites as a Function of Crystallization Temperature

Material	124		125		126		127		128	
	n	k ($\times 10^6$)	n	k ($\times 10^6$)	n	k ($\times 10^6$)	n	k ($\times 10^6$)	n	k ($\times 10^6$)
PP	2.3	8.7	2.4	2.1	2.4	1.4	2.4	0.41	2.4	0.27
PP 0.5 wt % MMT	2.2	16	2.2	10	2.2	6.4	2.2	3.8	2.3	1.0
PP 1.0 wt % MMT	2.0	98	2.0	63	2.0	32	2.0	13	2.11	4.8
PP 3.0 wt % MMT	1.9	190	1.8	180	1.8	120	1.9	68	1.9	29
PP 5.0 wt % MMT	1.8	640	2.1	600	2.2	430	2.0	76	2.2	16
PP(10% PP-*g*-MA) 5.0 wt % MMT	2.2	42	2.2	22	2.2	10	2.3	5.2	2.3	3.5
PP 5.0 wt % C30B	2.4	62	2.4	41	2.4	24	2.5	8.7	2.4	6.6
PP 5.0 wt % C10A	2.6	47	2.7	14	2.7	5.9	2.8	1.9	2.7	2.1

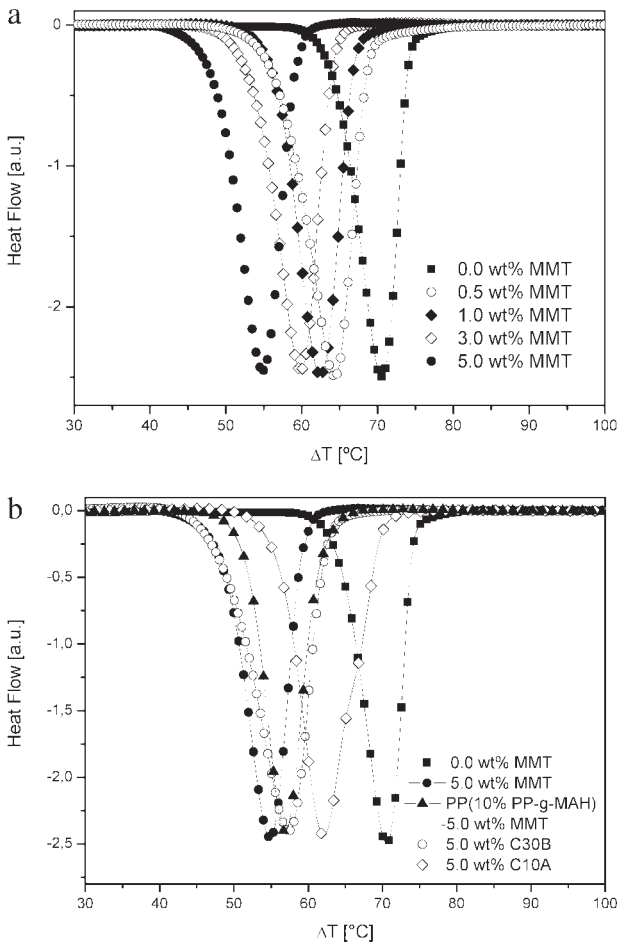

Figure 6 Heat flow as a function of the undercooling degree at 10°C/min for (a) matrix and nanocomposites with different MMT contents and (b) matrix and nanocomposites with modified initial materials: PP-5 wt % C30B; PP-5 wt % C10A; and PP(10% PP-*g*-MA)-5 wt % MMT.

slower crystallization process. So, this parameter (k) could be useful to understand the nucleation and fastening effect of clay and to elucidate the matrix/clay compatibility: a higher k value implies a higher nucleation effect, a lower matrix/clay compatibility, and lower clay dispersion degree.

k values demonstrated that the crystallization kinetics of nanocomposites is less temperature dependent than that of the matrix in the nucleus formation step.

Similar to nucleation process, the preexponential factors (k_0) and activation energies (E_a) were obtained from a typical nonlinear regression method. The results of activation energies (for an average k_0 of 1.4×10^{14}) are also included as Table IV. The addition of layered silicate into the matrix should cause more heterogeneous nucleation, so it is expected to obtain a lower E_a.

All the previous results should indicate that the matrix/clay compatibility (dispersion degree and intercalation-exfoliation ratio) is most important than

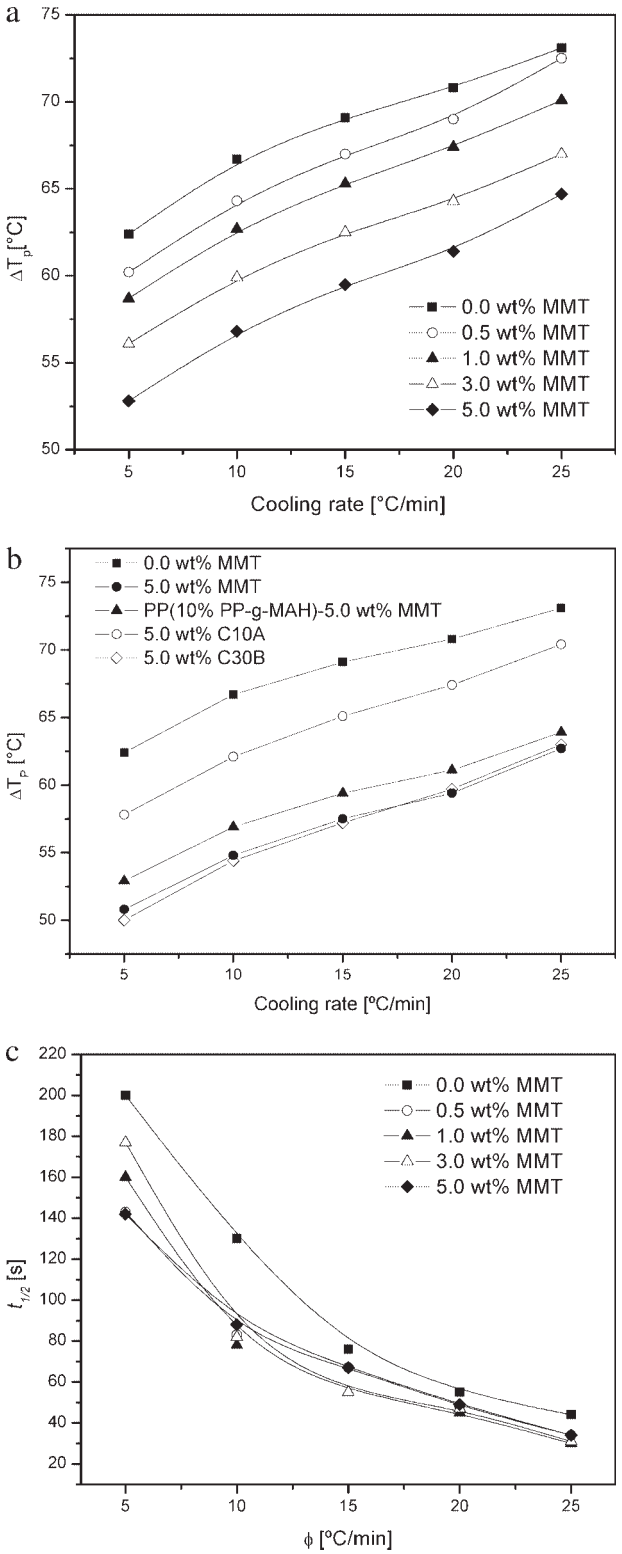

Figure 7 a) $\Delta T_p = T_m^0 - T_p$ as a function of cooling rate for (a) PP matrix and nanocomposites with different MMT contents; (b) $\Delta T_p = T_m^0 - T_p$ as a function of cooling rate for nanocomposites with modified initial materials: PP-5 wt % C30B; PP-5 wt % C10A; and PP(10% PP-*g*-MA)-5 wt % MMT; (c) nonisothermal half-crystallization time as a function of cooling rate for PP matrix and nanocomposites with different MMT contents.

TABLE VI
Parameters of Nonisothermal Crystallization for Different Studied Materials

	$\Delta T_{p\ 10°C/min}$ (°C)	$t_{1/2\ 10°C/min}$ (s)	E_a (kJ/mol)	ε	Ozawa		Avrami		Mo	
					$K(T)$	m	Z_c	n	b	$F(T)$
PP	66.7	130	228.2	1	160	2.9	0.380	5.3	1.18	22.2
PP 0.5 wt % MMT	64.3	83	213.6	0.82	300	2.2	0.389	4.9	1.20	18.2
PP 1.0 wt % MMT	62.7	78	200.2	0.80	420	2.3	0.331	5.3	1.08	18.2
PP 3.0 wt % MMT	59.9	82	210.1	0.73	1000	2.4	0.389	5.4	1.02	14.9
PP 5.0 wt % MMT	56.8	88	211.5	0.58	1520	2.2	0.371	5.2	1.27	16.4
PP (10% PP-*g*-MA)-5.0 wt % MMT	58.9	63	224.3	0.63	1290	2.3	0.468	4.3	1.15	12.2
PP 5.0 wt % C30B	57.4	76	185.1	0.60	410	2.3	0.436	4.2	1.16	18.2
PP 5.0 wt % C10A	62.1	92	192.0	0.71	490	2.2	0.468	4.1	1.22	13.5

$\Delta T_p = T_m^0 - T_p$, T_p: peak temperature at cooling rate of 10°C/min; $t_{1/2\ 10°C/min}$: half-crystallization time at cooling rate of 10°C/min; E_a: activation energy for the transport of the macromolecular segments to the growing surface (Kissinger method); ε: nucleation activity; Ozawa: parameters of Ozawa's model obtained at $T_c = 118$°C; Avrami: parameters of Avrami's model obtained at 20°C/min; Mo: parameters of Mo's model obtained for $\alpha = 0.6$.

the interlayer spacing (contact area between polymer segments and clay surface) to determine the nucleation and acceleration effect of the filler on the crystallization behavior of the PP matrix.

Nonisothermal crystallization analysis

The crystallization curves of matrix and nanocomposites at 10°C/min are shown in Figure 6. The addition of clay produced a faster crystallization process and a significant decrease on undercooling degree ($\Delta T_p = T_m^0 - T_p$), whose values are shown in Figure 7(a), because nanoparticles acted as effective nucleating agents. The last figure shows that, in all cases, ΔT_p increased with increased cooling rate. At lower cooling rates, there is more time to overcome the nucleation energy barriers and, so that, crystallization starts at higher temperatures, whereas as the cooling rate is raised, the nuclei became active at lower temperatures,[52] also conducting to smaller spherulites during the heterogeneous nucleation process. T_p and also $t_{1/2}$ for a cooling rate of 10°C/min are summarized in Table VI. As expected, the value of $t_{1/2}$ decreased with the increased cooling rates for matrix and nanocomposites [Fig. 7(c)]. It can be observed that for a fixed cooling rate, the half-crystallization times for nanocomposites were lower than for the neat PP implying that the addition of clay can accelerate the overall non-isothermal crystallization process.[4] The values of $\ln\left(\phi/T_p^2\right)$ were plotted as a function of $1/T_p$ and good relations were obtained; from these plots, the activation energy for the transport of the macromolecular segments to the growing surface was estimated and these values are included in Table V. The results of activation energies of nonisothermal melt crystallization (lower E_a for nanocomposites) also show the nucleating effect of nanoclay, as it was previously discussed. Other authors[8,16] have found a similar trend on activation energy. Even though the activation energy decreased from matrix to nanocomposites, it tends to increase as a function of clay content because of the increase on the melt viscosity due to the confinement effect of the clay on the motion of the polymer chains.[53]

Table V also includes the nucleation activity[31]; if the filler is extremely active for nucleation, ε approaches to zero, whereas for an absolutely inert particle it becomes 1. The nucleation activity values demonstrated that MMT is an effective nucleating agent for PP; moreover, that effect clearly increased with clay content (ε decreased); the silicate layers are active substrates for the heterogeneous nucleation of PP crystals, which decrease the free energy that oppose primary nucleation. This parameter was higher for nanocomposites with organoclays and also when 10 wt % of PP-*g*-MA was incorporated, indicating lower nucleation ability for higher polymer/matrix compatibility which is in accordance with the previous results of isothermal crystallization.

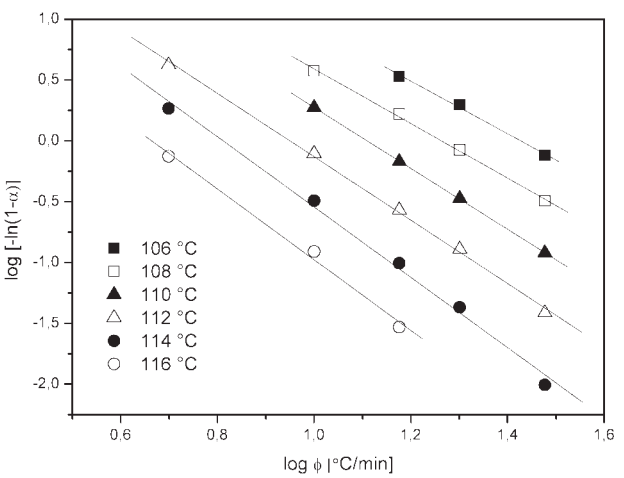

Figure 8 Ozawa plots, $\log(-\ln(1-\alpha))$ vs. $\log \phi$, for the nonisothermal crystallization of PP matrix.

TABLE VII
Ozawa's Parameters for the Nonisothermal of Pure PP and PP/MMT Nanocomposites

	PP		PP 0.5 wt % MMT		PP 1 wt % MMT		PP 3 wt % MMT		PP 5 wt % MMT	
T (°C)	m	$K(T)$	m	$K(T)$	m	$K(T)$	m	$K(T)$	m	$K(T)$
116	2.9	210	2.1	470	2.2	550	2.3	1480	2.2	2700
118	2.9	160	2.2	300	2.3	420	2.4	1000	2.2	1520
120	2.6	50	2.2	110	2.4	180	2.4	760	2.2	800

Although several authors have claimed that Ozawa's model was nonapplicable for the nonisothermal crystallization process because it ignores secondary crystallization,[5,6] other ones[54] have explained that during cooling, secondary crystallization could not take place because of the continuous decrease in temperature. So, we tried to use this approach in PP/MMT nanocomposites. Figure 8 shows the Ozawa plots for matrix. Similar ones were obtained for nanocomposites. As straight lines can be traced, the Ozawa analysis should be valid in this case. The parameters calculated from this analysis are shown in Table VII. The value of $K(T)$ increased as the crystallization temperature decreased (higher driving force for the crystallization process) for the matrix and also for all nanocomposites, but the values were higher for the nanocomposites than for the matrix at any given crystallization temperature (increasing with clay content) implying that nanocomposites crystallized faster than the pure matrix, which is also coincident with all previous results. A similar trend was found by Xu et al.[9] in the case of PP/PP-*g*-MA/Org-MMT. On the other hand, m had not a clear tendency with temperature but it was higher for matrix (2.8 ± 0.2) than for nanocomposites (2.0 ± 0.4), related also with the faster crystallization of the nanocomposites.

So that, both parameters $K(T)$ and n from Ozawa model's could show the nucleating effect of nanoparticles on the crystallization behavior of PP matrix.

An alternative approach was adopted by Avrami and the results for our systems are displayed in Table VIII. It is important to note that the parameters (Z_t and n) do no have the same physical meaning than in isothermal crystallization because under nonisothermal crystallization the temperature changes continuously affecting the nuclei formation and spherulite growth rate (which depend on the temperature). The corrected crystallization constant (Z_c) increased as a function of cooling rate, which is an expected behavior because it is an indication of the crystallization rate that gets faster under cooling. Nevertheless, a correlation between clay content and this parameter was not found, as in the case of PP-*g*-MA/MMT[20] at low cooling rates. Dissimilar results (increasing trend: Papageorgeou et al.[6]; Xu et al.[9] or decreasing trend: Li et al.[20]) have been found for this parameter by comparing nanocomposites and neat PP matrix. Although the changes in n did not show an apparent trend, it was smaller for the matrix than for the nanocomposites indicating that MMT nanoparticles acted as heterogeneous nuclei for the initial nucleation. A similar tendency was found in the case of PP/SiO_2 nanocomposites.[6]

The previous results seem to show that this model (Avrami) is not completely adequate to establish the correlations of the effect of nanofiller on the nonisothermal crystallization of PP matrix.

The combination of both previous models (Ozawa and Avrami) leads to Mo's analysis whose parameters are summarized in Table IX. The values of $F(T)$ increased with the relative degree of crystallinity (α), whereas no obvious tendency were observed as a function of clay content. Analyzing the effect of clay content at a fixed cooling rate (see Table V), it is clear that this parameter was slighter for nanocomposites than for the matrix indicating the heterogeneous nucleation effect of MMT.[16] The changes in b indicate that the presence of the nucleating agent

TABLE VIII
Avrami's Parameters for the Nonisothermal of Pure PP and PP/MMT Nanocomposites

ϕ	5		10		15		20		30	
Sample	n	Z_c	n	Z_c	n	Z_c	n	Z_c	n	Z_c
PP	4.8	0.009	4.9	0.120	5.0	0.263	5.3	0.380	5.5	0.537
PP 0.5 wt % MMT	5.1	0.004	4.9	0.100	4.9	0.245	4.9	0.389	4.7	0.562
PP 1 wt % MMT	6.3	0.001	6.0	0.063	5.5	0.214	5.3	0.331	5.0	0.549
PP 3 wt % MMT	5.7	0.002	5.1	0.102	4.9	0.269	5.4	0.389	4.8	0.575
PP 5 wt % MMT	4.8	0.003	5.8	0.071	6.5	0.214	5.2	0.372	5.4	0.525

TABLE IX
Mo's Parameters for the Nonisothermal of Pure PP and PP/MMT Nanocomposites

α	0.2		0.4		0.6		0.8	
Sample	*b*	*F*(*T*)	*b*	*F*(*T*)	*b*	*F*(*T*)	*b*	*F*(*T*)
PP	1.19	18.2	1.19	20.1	1.18	22.2	1.19	24.5
PP 0.5 wt % MMT	1.24	12.2	1.20	14.9	1.20	18.2	1.23	20.1
PP 1 wt % MMT	1.05	14.9	1.07	16.4	1.08	18.2	1.10	20.1
PP 3 wt % MMT	0.98	11.0	1.01	13.5	1.02	14.9	1.04	16.4
PP 5 wt % MMT	1.30	12.2	1.29	14.9	1.27	16.4	1.27	18.2

affect in a different way n compared with m. The values of b were always higher than 1 indicating that Avrami exponent was always higher than that of the Ozawa. $F(T)$ values increased with the degree of crystallinity, whereas at a certain degree of crystallinity they remained almost unaffected by the presence of the clay, as previously reported by Papageorgiou et al.[6] So, although this last model correctly represents the experimental crystallization curves for the matrix and nanocomposites, the parameters do not appear to be good to establish the nucleating effect of the clay.

Spherulitic growth

Figure 9 shows growing spherulites micrographs for PP at the undercooling degree of 42°C at two different times (180 and 420 s). The morphology of all the studied spherulites (not shown) was quite similar. Table X summarizes the spherulites radius and the number of growing nucleus at the same time and undercooling degree for matrix and selected nanocomposites. A decreasing trend on spherulites radius as a function of MMT content can be observed, which is related to their nucleating effect.[55] On the other hand, it can be noted that at same time, the number of growing nucleus augment with the clay content, this fact can also be attributed to the nucleating effect of the clay particles, which in turn coincides with the studies carried out by DSC. Both parameters (number of nucleus and spherulites radius) also show the lower nucleating ability of the modified clay because of its higher compatibility with the matrix.

The spherulites radius as a function of time for the matrix and nanocomposites at the same undercooling degree are displayed in Figure 10(a). At least eight spherulites were measured for each test. The spherulite radius increased linearly with the time in all cases. This behavior was observed at all undercooling degrees and indicates that the growth rate is independent of the spherulites size. From the previous figure, the spherulitic growth rate was calculated as $G = dR/dt$ which is the slope of the experimental radius versus time curve at each temperature. The obtained values at $T_c = 140$°C are also included in Table IX.

The spherulitic growth rate increased as a function of MMT content. Comparing nanocomposites with 5 wt % of different clays (MMT and C10A); the last one shows a slower spherulitic growth that can be related to the major compatibility with the matrix. Additionally, in all cases, the growth rate increased with the undercooling degree. The obtained values were correlated [Fig. 10(b)] by using spherulitic growth equation (see Table I).

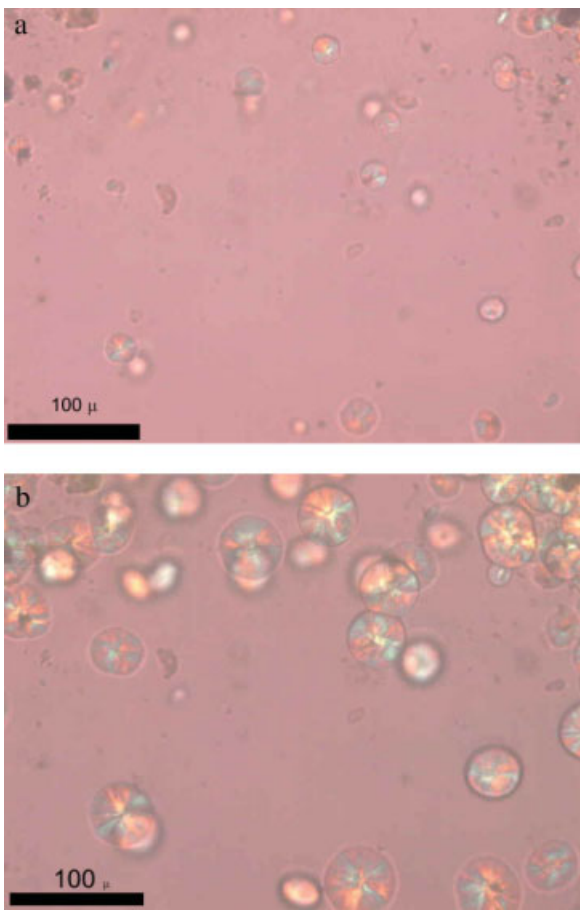

Figure 9 Spherulites morphology of PP matrix crystallized at 140°C for different times: (a) 180 and (b) 420 s. [Color figure can be viewed in the online issue, which is available at www.interscience.wiley.com.]

TABLE X
Parameters of Spherulitic Growth

Sample	Growing nucleus number × mm^2 (140°C, 420 s)	Spherulites radius (μm) (140°C, 420 s)	G (μm/s) (140°C)	G_0 (μm/ s)	K_g
PP	136 ± 35	62.6 ± 8.2	0.13	3.09×10^5	7.6×10^4
PP-3 wt % MMT	264 ± 23	41.5 ± 5.1	0.16	2.04×10^4	5.4×10^4
PP-5 wt % MMT	378 ± 57	19.7 ± 2.1	0.18	6.61×10^2	2.9×10^4
PP-5 wt % C10A	235 ± 35	57.2 ± 6.2	0.10	1.74×10^5	7.3×10^4

K_g and G_0 calculated on this way are also summarized in Table IX. K_g decreased as the clay was incorporated, because of the action of the clay as nucleation agent. In the case of the nanocomposites with 5 wt % of C10A, the value is lower due to the increased compatibilization. So that, K_g could be used to analyze the nucleation effect of the clay on the spherulitic growth of PP matrix and also to analyze the matrix/clay compatibility (and with the intention of inferring the dispersion of the clay platelets inside the matrix).

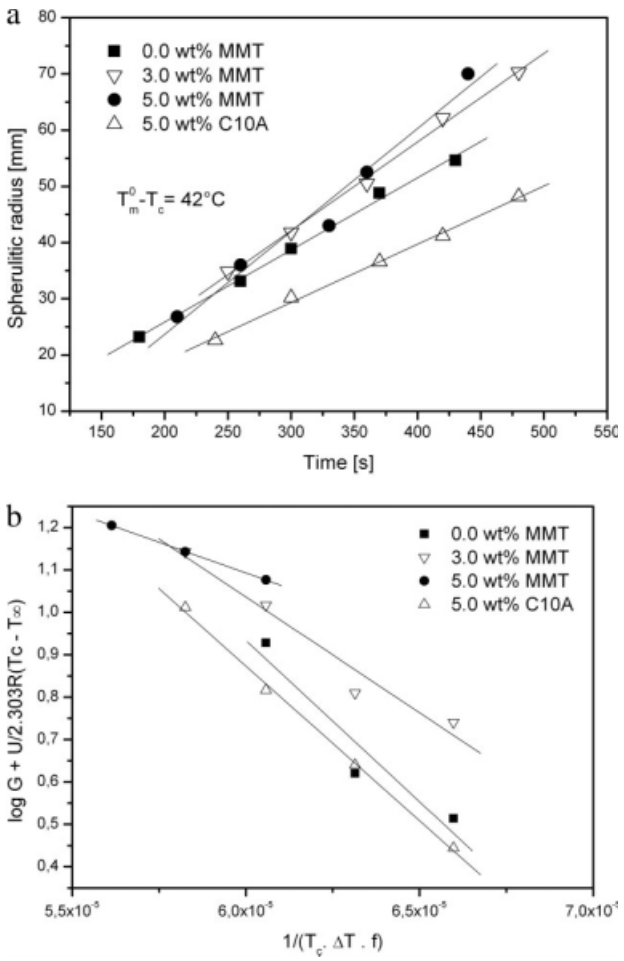

Figure 10 (a) Spherulites radius as a function of time for the matrix and several nanocomposites at 140°C and (b) modeling of spherulitic growth.

CONCLUSIONS

The effect of clay nanoparticles and matrix/clay compatibility on the bulk crystallization and spherulitic growth behavior of PP was studied.

All results (experimental and models parameters) demonstrated that clay nanoparticles acted as nucleating agents and that this ability can be directly correlated to the matrix/clay compatibility (dispersion degree and intercalation–exfoliation ratio) being lower for the higher interaction.

From the used models, Ozawa parameters seem to show this nucleating effect of nanoparticles on the crystallization behavior of PP matrix, whereas Avrami and Mo models seem to be not completely adequate to determine this effect.

In addition, the nucleation activity, ε and also K_g look like interesting parameters to determine the nucleating effect of the nanoparticles on the crystallization behavior of PP matrix and also to infer correlations with the clay dispersion degree, i.e., the higher the matrix–clay compatibility, the higher are both parameters.

References

1. Di Maio, E.; Iannace, S.; Sorrentino, L.; Nicolais, L. Polymer 2004, 45, 8893.
2. Homminga, D.; Goderis, B.; Dolbnya, I.; Groeninckx, G. Polymer 2006, 47, 1620.
3. Liu, X.; Wu, Q. Polymer 2001, 42, 10013.
4. Jain, S.; Goossens, H.; Van Duin, M.; Lemstra, P. Polymer 2005, 46, 8805.
5. Yuan, Q.; Awate, S.; Misra, R. D. K. Eur Polym J 2006, 42, 1994.
6. Papageorgiou, G.; Achilias, D.; Bikiaris, D.; Karayannidis, G. Thermochim Acta 2005, 427, 117.
7. Medellin-Rodriguez, F. J.; Mata-Padilla, J. M.; Hsiao, B. S.; Waldo-Mendoza, M. A.; Ramirez-Vargas, E.; Sánchez-Valdes, S. Polym Eng Sci 2007, 47, 1889.
8. Xu, W.; Ge, M.; He, P. J Polym Sci Part B: Polym Phys 2002, 40, 408.
9. Xu, W.; Liang, G.; Zhai, H.; Tang, S.; Hang, G.; Pan, W. Eur Polym J 2003, 39, 1467.
10. Yuan, Q.; Misra, R. D. K. Polymer 2006, 47, 4421.
11. Li, J.; Zhou, C.; Wang, G.; Tao, Y.; Liu, Q.; Li, Y. Polym Test 2002, 21, 583.
12. Prakashan, K.; Gupta, A. K.; Maiti, S. N. J Appl Polym Sci 2008, 108, 1298.
13. Krikorian, V.; Pochan, D. J. Macromolecules 2004, 37, 6480.

14. Svoboda, P.; Zeng, C.; Wang, H.; Lee, J.; Tomasko, D. L. J Appl Polym Sci 2002, 85, 1562.
15. Yang, K.; Yang, Q.; Li, G.; Sun, Y.; Feng, D. Mater Lett 2006, 60, 805.
16. Wang, L.; Sheng, J. J Macromol Sci Phys 2005, 44, 31.
17. Ma, J.; Zhang, S.; Qi, Z.; Li, G.; Hu, Y. J Appl Polym Sci 2002, 83, 1978.
18. Ning, N.; Yin, Q.; Luo, F.; Zhang, Q.; Du, R.; Fu, Q. Polymer 2007, 48, 7374.
19. Burke, M.; Young, R. J.; Stanford, J. L. Polym Bull 1993, 30, 361.
20. Li, J.; Zhou, C.; Gang, W. Polym Test 2003, 22, 217.
21. Kennedy, M.; Brown, G. R.; St. Pierre, L. E. Polym Eng Sci 1990, 30, 769.
22. Kennedy, M.; Brown, G. R.; St. Pierre, L. E. Polym Compos 1984, 5, 307.
23. Yam, W. Y.; Ismail, J.; Kammer, H. W.; Schmidt, H.; Kummerlöwe, C. Polymer 1999, 40, 5545.
24. Lin, C. C. Polym Eng Sci 1983, 23, 113.
25. Avrami, M. J Chem Phys 1939, 7, 1103.
26. Avrami, M. J Chem Phys 1940, 8, 212.
27. Hoffman, J. D.; Davis, G. T.; Lauritzen, J. I. In Treatise on Solid State Chemistry; Hannay N.B., Ed.; Plenum Press: New York, 1976; Vol. 3, Chapter 7, p 497.
28. Janevsky, A.; Bogoeva-Gaceva, G. J Appl Polym Sci 1998, 69, 381.
29. Hoffnam, J. D. Polymer 1982, 23, 656.
30. Cebe, P.; Hong, S. D. Polymer 1986, 27, 1183.
31. Dobreva, A.; Gutzow, I. J Non-Cryst Solids 1993, 162, 13.
32. Jeziorny, A. Polymer 1978, 19, 1142.
33. Ozawa, T. Polymer 1971, 12, 150.
34. Liu, T. X.; Mo, Z. S.; Wang, S. E.; Zhang, H. F. Polym Eng Sci 1997, 37, 568.
35. Kisinger, H. E. J Res Nat Inst Stand Technol 1956, 57, 217.
36. Borsig, E.; Ujhelyiová, A.; Mlynarcíková, Z.; Kaemfer, D.; Mülhaupt, R.; Marcincin, A.; Berek, D. Int J Polym Mater 2007, 56, 771.
37. Li, J.; Ton-That, M.-T.; Leelapornpisit, W.; Utracki, L. A. Polym Eng Sci 2007, 47, 1447.
38. Jiang, S.; Ji, X.; An, L.; Jiang, B. Acta Polym Sinica 2000, 4, 452.
39. Cheng, Y.; Xu, M. Acta Polym Sinica 1998, 5, 671.
40. Iannace, S.; Nicolais, L. J Appl Polym Sci 1997, 64, 911.
41. De Rosa, C.; Auriemma, F.; Vinti, V.; Galimberti, M. Macromolecules 1998, 31, 6206.
42. Yamada, K.; Hikosaka, M.; Toda, A.; Yamazaki, S.; Tagashira, K. Macromolecules 2003, 36, 4790.
43. Maiti, P.; Nam, P. H.; Okamoto, M.; Hasegawa, N.; Usuki, A. Macromolecules 2002, 35, 2042.
44. Seo, Y.; Kim, J.; Kim, K. U.; Kim, Y. C. Polymer 2000, 41, 2639.
45. Kawasami, M.; Hasegawa, N.; Kato, M.; Usuki, A.; Okada, A. Macromolecules 1997, 30, 6333.
46. Nam, P. H.; Maiti, P.; Okamoto, M.; Kotaka, T.; Hasegawa, N.; Usuki, A. Polymer 2001, 42, 9633.
47. Kato, M.; Usuki, A.; Okada, A. J Appl Polym Sci 1997, 66, 1781.
48. Dennis, H. R.; Hunter, D. L.; Chang, D.; Kim, S.; White, J. L.; Cho, J. W. Polymer 2001, 42, 9513.
49. Tarapow, J.; Bernal, C.; Alvarez, V. J Appl Polym Sci 2009, 111, 768.
50. Ludueña, L.; Alvarez, V.; Vazquez, A. J Appl Polym Sci 2008, 109, 3148.
51. Reinsch, V. E.; Rebenfeld, L. J Appl Polym Sci 1994, 52, 649.
52. Di Lorenzo, M. L.; Silvestre, C. Prog Polym Sci 1999, 24, 917.
53. Michael, J. S.; Abdulawahab, S. A.; Kurt, F. S.; Anongnat, S.; Priya, V. Macromolecules 2001, 34, 1864.
54. Lopez, L. C.; Wilkes, L. G. Polymer 1989, 30, 882.
55. Wang, L.; Sheng, J.; Wu, S. J Macromol Sci Phys 2005, 43, 935.